Journal of Environmental Chemical Engineering 7 (2019) 102817

Contents lists available at ScienceDirect

Journal of Environmental Chemical Engineering

journal homepage: www.elsevier.com/locate/jece

# Surface enriched nanofiber mats for efficient adsorption of Cr(VI) inspired by nature

Sara Mousavi[a,b], Farhad Shahraki[b,*], Majid Aliabadi[c], Aminoddin Haji[d], Fabian Deuber[a], Christian Adlhart[a,*]

[a] Institute of Chemistry and Biotechnology, Zurich University of Applied Sciences ZHAW, 8820 Wädenswil, Switzerland
[b] Department of Chemical Engineering, University of Sistan and Baluchestan, Zahedan, Iran
[c] Department of Chemical Engineering, Birjand Branch, Islamic Azad University, Birjand, Iran
[d] Department of Textile Engineering, Yazd University, Yazd, Iran

ARTICLE INFO

*Keywords:*
Nanofibers
Fixed bed column
Adsorption isotherms
Filtration
Thermodynamics
BET surface area

ABSTRACT

Adsorption is a surface process. By evolution, nature has created design principles such as scaffolds that allow to carrying surface bound agents at high density. We used a nanofibrous pullulan/poly(vinyl alcohol)/poly(acrylic acid) (Pul/PVA/PAA) support to carry surface active PAMAM dendrimer similar to spores attached to mushroom gills. A monolayer of ceria ($CeO_2$) nanoparticles served as the linker between PAMAM and the nanofiber. The nanocomposite was a highly effective Cr(VI) adsorbent and the maximum adsorption capacity $q_{max} = 847\ mg\ g^{-1}$ is the highest reported value for the same kind of materials so far. The materials was characterized by scanning electron microscopy (SEM), thermogravimetric analysis (TGA), Fourier transform-infrared spectroscopy (FTIR), zeta potential and multipoint BET method to measure the specific surface area. Removal of Cr(VI) from aqueous media was tested under different batch and fixed bed column operation conditions such as pH, temperature and competing ions. Thermodynamic properties were determined based on a modified Langmuir adsorption isotherm and the adsorption kinetic was investigated. Positive entropy of adsorption and an endothermic adsorption process was found, while the rate-limiting step was pseudo second order which is associated with a chemisorption process. The nanocomposite was reusable and up to 95% of the adsorbed Cr(IV) ions were recovered by alkyne washing.

## 1. Introduction

Nowadays, detoxification of various pollutants from wastewaters is a challenging issue in water treatment and environmental protection processes. Presence of heavy metals and hexavalent chromium in particular is one of the most important issues. Therefore they are an extensively studied target pollutant [1]. The widespread use of Cr(VI) in various industries such as metallurgy (steel, ferro and nonferrous alloys), chemistry (pigments, electroplating, tanning and other) and refractories (chrome and chrome- magnesite) [2,3], gives the chromium removal process a big priority in water treatment. According to previous studies using different removal methods, adsorption is still the best and most popular method due to being cheap, easily controlled, and highly efficient [4,5].

Recently, different investigations introduced nano-sized metal oxides such as iron oxide, manganese oxides, aluminium oxides, titanium oxides, and cerium oxides as promising adsorbents for the removal process of heavy metals from aqueous systems [6–9]. The most important reason of using nano-structured metal oxides is their large specific surface area [10]. Many studies showed that nano-sized metal oxides are favorable adsorbents for heavy metals due to their high capacity and selectivity [6,11]. However, reducing the size of metal oxides to nanometer increases the surface energy which leads to a very poor stability and very high agglomeration tendency in the presence of van der Waals forces or other electrostatic interactions [12]. Since agglomeration has a great negative effect on adsorption capacity, finding an efficient support for stabilizing of nanoparticles is very important.

Electrospun nanofibers are promising and widely used materials in a vast variety of fields such as water treatment - in particular the heavy metal removal processes - due to a high surface area and their porous structure [4,13–23]. Using electrospun nanofibers as a support for nanoparticles could result in providing a nanocomposite with advantages of both materials. Recently, this approach has been investigated using different polymers for nanofiber synthesis as well as different

* Corresponding authors.
*E-mail addresses:* fshahraki@eng.usb.ac.ir (F. Shahraki), christian.adlhart@zhaw.ch (C. Adlhart).

https://doi.org/10.1016/j.jece.2018.102817
Received 28 September 2018; Received in revised form 19 November 2018; Accepted 1 December 2018
Available online 05 December 2018

nanoparticles [4,24,25]. Such combined materials do not only provide an efficient adsorbent for the heavy metal removal process, but the separation of the adsorbent from the filtrate is easy and convenient without the necessity of using any further method.

Organic functional groups such as amines show favorable interactions with heavy metals due to their ability to coordinate ions [9,24,26–32]. In this work, we were able to modify the surface of nanoparticles attached to a nanofibrous support with the help of highly branched polyamidoamine (PAMAM) dendrimer macromolecules. For this purpose, environmentally friendly nanofibers were produced by electrospinning using a mixture of pullulan, polyvinyl alcohol, and poly acrylic acid. The nanofibers were coated with cerium oxide nanoparticles followed by surface modification with the dendrimer. The nanocomposite provided a high amount of amine groups and consequently it was a super active adsorbent for Cr(VI) removal.

## 2. Experimental

### 2.1. Materials

Cerium (IV) oxide ($CeO_2$-NPs) (nano powder, < 25 nm), (3-glycidyloxypropyl) trimethoxysilane (> 98%) (GPTMS), PAMAM dendrimer with ethylene diamine core, generation 3.0 solution (20 wt% in methanol), poly(vinyl alcohol) (PVA, Mw = 89,000–98,000 Da, DH = 99%), poly(acrylic acid) sodium salt (PAA, Mw = 5100), NaOH (sodium hydroxide), HCl (hydrochloric acid, ACS reagent 37%), 1,5-diphenylcarbazide (ACS reagent), sulfuric acid (95–98 %), $NaNO_3$ (sodium nitrate), $KH_2PO_4$ (potassium hydrogen phosphate), $Na_2SO_4$ (sodium sulfate), and $K_2Cr_2O_7$ (potassium dichromate, ACS reagent, > 99%) were bought from Sigma Aldrich, Germany. Pullulan (food grade) (Pul) was provided by Hayashibara Co. Ltd., Japan. Scheme 1a and b show the structure of the polymers and the dendrimer.

### 2.2. Preparation of electrospun nanofibers (NF)

Electrospinning solution was prepared by dissolving 14.5% mass fraction of Pul/PVA/PAA (ratio 2:3:2) in distilled water. The nanofibers were electrospun using a Nanospider™ NS lab 500 (Elmarco s.r.o., Czech Republic). A high voltage of 78 kV was used on the system with a cylindrical electrode and backing paper as collector. The distance between electrode and collector was 19 cm. Temperature and humidity during electrospinning was 27 ± 3 °C and 26 ± 4% respectively resulting in uniform nanofiber production. Nanofiber mats were then thermally crosslinked at 180 °C for 15 min in air to become water insoluble [16–19].

### 2.3. Preparation of ceria coated nanofibers ($CeO_2$/NF)

Cerium oxide (Ceria) suspension was prepared by sonication of $CeO_2$-NPs in deionized water (2 g $l^{-1}$) for 3 min followed by dipping the neat nanofiber mats in it for 30 s (5 g nanofibers in 1 l suspension). The coated nanofibers were rinsed three times with deionized water and dried at 50 °C for 2 h. The optimum conditions were identified using different concentrations and treatment time and nicely covered nanofibers without any agglomeration of nanoparticles were obtained based on SEM images.

### 2.4. Synthesis of dendrimer/ceria nanocomposite with nanofibrous support (D/$CeO_2$/NF)

About 350 mg $CeO_2$/NF were stirred in 100 ml of ethanol for 20 min, followed by addition of 100 µl of GPTMS to the solution. GPTMS as a reactive silane coupling agent was used due to its capacity for making stable chemical bonds between inorganic (cerium oxide) and organic (dendrimer) materials [26,33–35]. The solution was stirred for 5 h at room temperature and the nanofibers were washed 3 times using ethanol and deionized water for removing unreacted GPTMS. Approximately 350 mg of surface treated nanofibers were stirred in a mixture containing 100 ml ethanol and 30 µl of dendrimer for 24 h at 45 °C. The chemically modified nanofibers were collected, washed 5 times with ethanol and deionized water and air dried. Scheme 1b is illustrating the synthetic procedure indicating that the chemically modified nanocomposite has high amount of active amine groups on the surface.

### 2.5. Preparation of dendrimer treated ceria nanoparticles (D/$CeO_2$)

Dendrimer treatment was also done for ceria nanoparticles to compare their adsorption efficiency with D/$CeO_2$/NF. 1 g of ceria nanoparticles were sonicated for 1 h in 100 ml of ethanol. Sonication was continued for 5 h after adding 1 ml of GPTMS to the mixture. The silanized nanoparticles were removed from unreacted GPTMS by centrifugation and washed three times with ethanol and water. About 1 g of surface modified nanoparticles were dispersed in a mixture of 150 ml of ethanol and 100 µl of PAMAM dendrimer and sonicated for 6 h at 50 °C. The chemically modified ceria nanoparticles were collected by centrifugation and dried at room temperature for one day (Scheme 1c).

### 2.6. Characterization

The morphology of the nanofibers was studied using a FEI Quantum FEG250 scanning electron microscope (SEM) with an acceleration voltage of 5 kV. The samples were gold coated (Quorum Q150RS sputter) for 30 s at 20 mA to prevent the charging effect during the measurements. The nanofiber diameter was determined manually from SEM images as suggested by Stanger et al. [36]. Transmission Fourier transform infrared spectroscopy (FTIR) experiments were performed at room temperature on a Bruker Tensor 37 instrument which was equipped with a pallet holder. For all the measurements, a pellet of the sample mixture with dried potassium bromide in 1:60 mass ratio was used. All spectra were collected between 400 and 4000 $cm^{-1}$ with a resolution of 4 $cm^{-1}$. Thermogravimetric analysis (TGA) was carried out using a Mettler Toledo (TGA 1 STAR e System) thermal gravimetric analyzer at a heating rate of 10 °C $min^{-1}$ in the range of 30 °C–1000 °C under nitrogen flow. The specific surface area, $a_{BET}$, of the adsorbent was determined by nitrogen sorption at 77 K with a Quantachrome Autosorb iQ MP instrument using the multipoint Brunauer- Emmett-Teller (BET) method. The theoretical surface area, $a_{calc}$, was calculated from geometric models with the assumption of cylindrical infinite fibers and spherical particles using Eqs. (1) and (2),

$$a_{calc}\ (\text{fibers}) = \frac{2V}{r} \quad (1)$$

$$a_{calc}(\text{nanoparticles}) = \frac{3V}{r} \quad (2)$$

where $V$ and $r$ are the volume and the radius of the fibers or nanoparticles, respectively. For the treated nanofiber samples ($CeO_2$/NF and D/$CeO_2$/NF), the theoretical surface area was calculated considering the amount of ceria and dendrimer treated ceria (D/$CeO_2$) on the surface (extracted from TGA results) with the assumption that the available surface of the nanofiber immobilized nanoparticles was half to surface of the nanoparticle sphere. Zeta potential and size of the nanoparticles were measured three times using dynamic light scattering (Malvern zetasizer Nano ZS). For the nanocomposite, the MütekTM SZP-06 device was used to determine the electrokinetic surface potential (zeta potential) of the nanofiber surfaces [37]. The pH of the solutions was adjusted using HCl and NaOH. The total amount of nitrogen (TN) on the surface of D/$CeO_2$/NF was balanced based on the unreacted dendrimer used in the preparation of D/$CeO_2$/NF (initial and final dendrimer containing solutions). The TN in the dendrimer solutions was determined using a Shimadzu TOC-L equipped with TNM-L

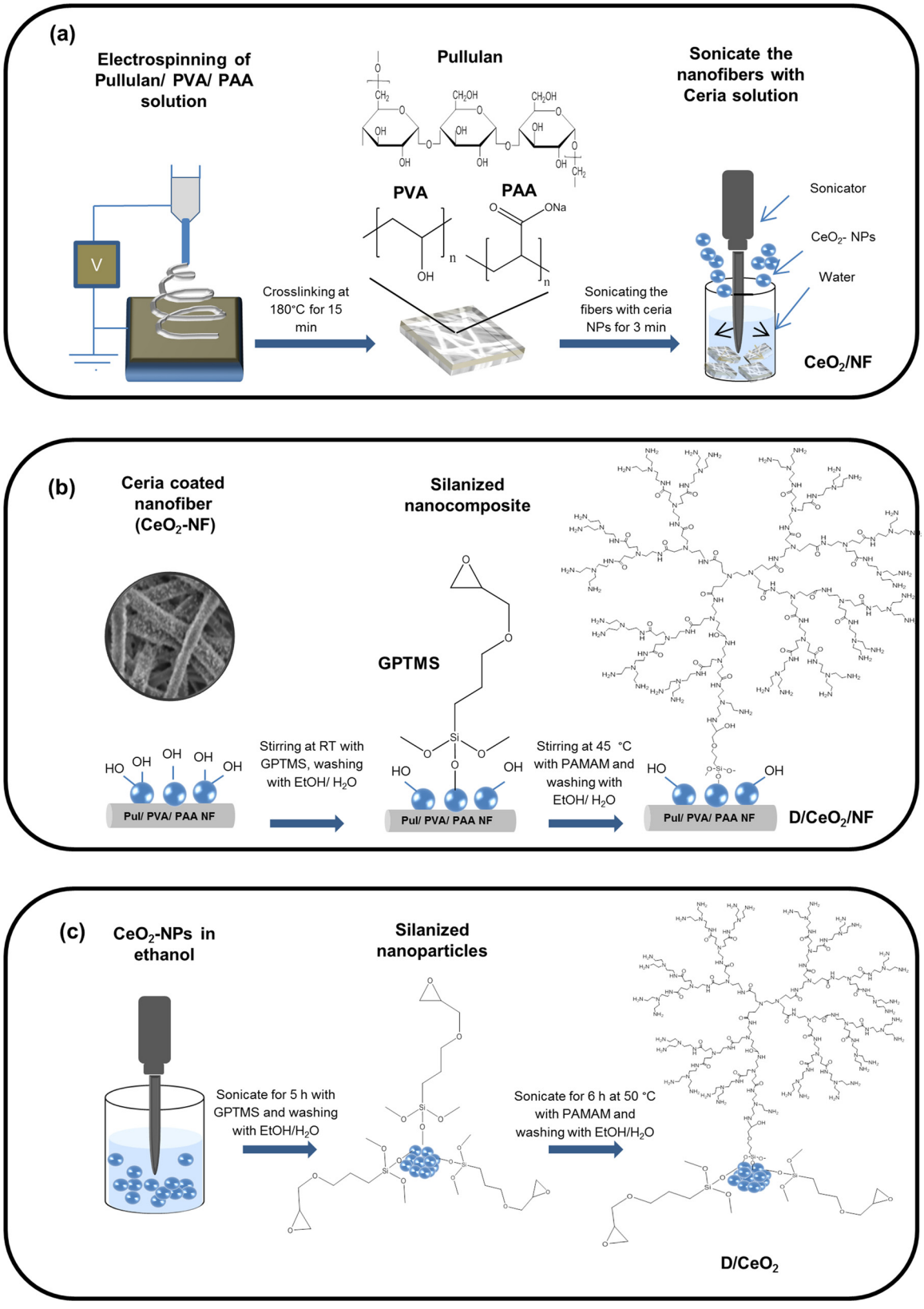


**Scheme 1.** Synthesis of (a) $CeO_2$/NF, (b) D/$CeO_2$/NF, and (c) D/$CeO_2$.

accessory (720 °C catalytic thermal decomposition/chemiluminescence method).

### 2.7. Batch adsorption experiments

A series of batch Cr(VI) adsorption experiments were carried out as functions of Cr(VI) initial concentration (1–900 mg $l^{-1}$), pH (1–12) and temperature (25 °C – 85 °C). Cr(VI) solutions were prepared by dissolving the corresponding amount of $K_2Cr_2O_7$ in deionized water. The initial pH was adjusted using 0.1 mol $l^{-1}$ HCl or 0.1 mol $l^{-1}$ NaOH solutions. The adsorbent amount was kept constant during the experiments (approx. 0.16 g $l^{-1}$) and the solution was stirred continuously at 300 rpm at room temperature for 8 h. Samples were taken at different time intervals and the Cr(VI) concentration was determined using UV–vis spectroscopy (Specord S 600, Analytik Jena, Germany) at $\lambda_{max}$ = 540 nm with diphenylcarbazide in acidic solution according to the standard colorimetric method used for the examination of water and wastewater [38]. The limit of quantification (95%, $f$ = 9) was determined to be 0.60 mg $l^{-1}$ and the sensitivity was 0.30 ± 0.01 l $mg^{-1}$, see also Fig. S1, Supporting information. The adsorption capacity of the nanocomposite at time $t$ was calculated according to Eq. (3):

$$q_t = \frac{\gamma_0 - \gamma_t}{m} V \quad (3)$$

Where $\gamma_0$ and $\gamma_t$ (mg $l^{-1}$) are the initial and time $t$ mass concentration of Cr(VI) in the solution, $q_t$ (mg $g^{-1}$) is the adsorption capacity at time $t$, $m$ (g) is the adsorbent dose and $V$ (l) is the volume of the solution. The mass concentration of saturated Cr(VI) in the bulk phase at pH 3, $\gamma_s$ (mg $g^{-1}$), was determined at the respective temperatures based on the dissolved mass of $K_2Cr_2O_7$ in a saturated filtrate.

To investigate the effect of other ions on adsorption, $NaNO_3$, $KH_2PO_4$, and $Na_2SO_4$ were added as representative materials at a respective concentration of 0.05 mol $l^{-1}$ to 300 ml of Cr(VI) solution ($\gamma$ = 50 mg $l^{-1}$) and stirred for 8 h in the presence of 50 mg of D/$CeO_2$/NF and the remaining mass concentration of Cr(VI) was determined.

Regeneration experiments were conducted separately using 1 mol $l^{-1}$ $HNO_3$, 0.1 mol $l^{-1}$ NaOH solutions, and deionized water with pH = 7. Afterwards, they were washed two times with deionized water and dried at room temperature.

### 2.8. Continuous adsorption experiments

For continuous adsorption experiments, one to three layers of NF and D/CeO2/NF were placed custom made fixed bed column with 15 mm diameter that was inspired by the design of industrial filter press used for plate filters in depth filtration, see Fig. S2. The mass of active adsorbent was 1.83 mg per layer. The feed rate was $\dot{V}$ = 2.8 ml $min^{-1}$ and the mass concentration of the solution was $\gamma_0$(Cr(VI)) = 5 mg $l^{-1}$. Samples were taken every minute until saturation of the adsorbent was achieved.

### 2.9. Statistics

Thermodynamic and kinetic parameters are given with a 95% confidence interval and the fit quality is expressed in terms of the coefficient of determination ($R^2$), the root mean square deviation (*RMSD*), and the relative root mean square deviation (*RRMSD*), see Supporting information and Tables S1–S3.

## 3. Results and discussion

### 3.1. Synthesis and characterization of $CeO_2$/NF, D/$CeO_2$, and D/$CeO_2$/NF

Dendrimer treatment of both ceria nanoparticles ($CeO_2$-NPs) and ceria coated nanofibers ($CeO_2$/NF) was done as illustrated in Scheme 1. The morphology of Pul/PVA/PAA nanofibers (NF) together with $CeO_2$/NF and D/$CeO_2$/NF was investigated by SEM images as presented in Fig. 1. Sonication is an efficient way to introduce a layer of nanoparticles to the nanofibrous support without any agglomeration (Fig. 1b). However, during the dendrimer treatment process partial adhesion between the nanofibers took place (Fig. 1c) which can be related to the high cross-linking that happened during the silanization and dendrimer treatment process due to different active methyl groups of GPTMS as well as to the huge amount of active amine groups of the PAMAM dendrimer that can attach to more than one $CeO_2$-NP surfaces at the same time. On the other hand, swelling of the fibers due to physical incorporation of dendrimer is significant (Figs. S3 and S4). The modification of the nanofiber surface was also followed by FTIR, Fig. 2a. The NF spectra exhibited absorption peaks of stretching vibrations at 3390 $cm^{-1}$ (O—H), 1720 $cm^{-1}$ (C═O) and 1020 $cm^{-1}$ (C—O). Comparing D/$CeO_2$/NF nanocomposite with NF and $CeO_2$-NPs with D/$CeO_2$, it is obvious that dendrimer treatment procedure introduced additional vibrations at 3270 $cm^{-1}$ (shoulder), 1660 $cm^{-1}$, and 1560 $cm^{-1}$ corresponding to the free and hydrogen bonded amide (CONH) and amine groups present in PAMAM dendrimer structure [39]. The amount of PAMAM dendrimer on D/$CeO_2$/NF was calculated from the total nitrogen and found to be 599 mg $g^{-1}$. The specific BET surface area of the nanofibers was 3.6 $m^2$ $g^{-1}$, Table 1. This is close to the calculated specific surface, which was derived from simple geometric models based on the nanofiber diameter (5.3 $m^2$ $g^{-1}$). Previous studies report specific BET surface areas of other electrospun nanofibers in a range between 0.6 and 33 $m^2$ $g^{-1}$ [40,41]. Covering the surface of nanofibers with a uniform thin layer of $CeO_2$-NPs increased the surface area of nanocomposite up to 46% which was decreased again after dendrimer treatment (from 5.3 $m^2$ $g^{-1}$ for $CeO_2$/NF to 5.0 $m^2$ $g^{-1}$ for D/$CeO_2$/NF). The magnified images of nanofibers show a rough surface morphology after attaching the $CeO_2$-NP. The size of the surface $CeO_2$-NP clusters was determined to be 139 nm by dynamic light scattering (DLS), which matches the observed roughness well. Interestingly, the BET surface area of the dry particles was 45.6 $m^2$ $g^{-1}$. This would give a BET based particle diameter of 18.2 nm which is within the specification of the supplier (< 25 nm). The calculated specific surface area based on the DLS diameter assuming a spherical model on the other hand is too low (6.0 $m^2$ $g^{-1}$) which indicates non-spherical particles and agglomeration, as was also observed by DLS (Fig. S5). For the free nanoparticles, the specific surface area is reduced by dendrimer treatment from 45.6 to 38.8 $m^2$ $g^{-1}$. This can be related to reducing the surface roughness of the particles as well as to a higher diameters due to dendrimer coating [42]. The BET measurements implied no positive effect of dendrimer treatment on the specific surface area of $CeO_2$-NPs and D/$CeO_2$/NF in the dry state. In the wet state, however, most of the nitrogen functional groups of the PAMAM dendrimer should be accessible for the adsorption of Cr(VI). TGA measurements are also presented in Fig. 2b. Untreated NF showed two main decomposition peaks related to the decomposition of the side and main chains of the polymeric nanofibers. However, covering nanofibers with $CeO_2$-NPs resulted in retarding the degradation process which is attributed to the reduced mobility of polymeric chains that are interacting through hydroxyl groups with the $CeO_2$-NPs. The residue on ignition of $CeO_2$/NF is 29.2% which is much higher than the observed 1.46% for the NF. The difference is related to the deposited $CeO_2$–NPs on the nanofiber surface. The amount of cerium oxide in each sample is presented in Table 1. The electric charge of nanocomposite as well as nanoparticles were measured in solution at different pH as illustrated in Fig. 2c. The nanofiber with an isoelectric point (IEP) around pH = 3.5 showed a big shift to an IEP at pH = 7.8 after dendrimer treatment due to the presence of amine groups on the surface of D/$CeO_2$/NF. The presence of cationic dendrimer causes the shift in IEP of nanoparticle as well (from pH = 7 to pH = 8.8). The same results are reported in other studies [27]. The possibility of agglomeration was investigated by measuring the size of the nanoparticles at different time intervals of sonication and a high agglomeration tendency of free nanoparticles was observed as shown

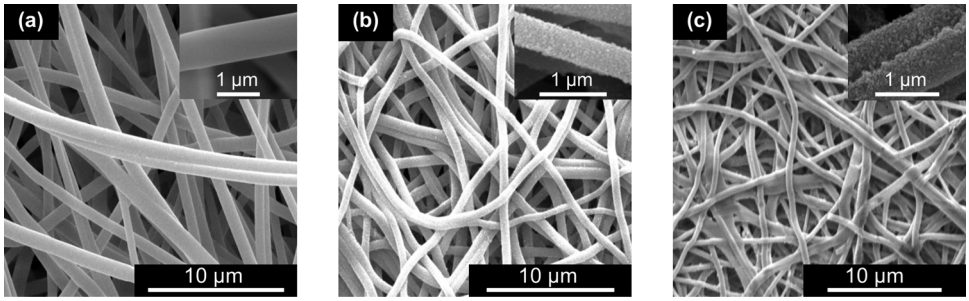


**Fig. 1.** SEM images of (a) NF, (b) $CeO_2$/NF, and (c) D/$CeO_2$/NF.

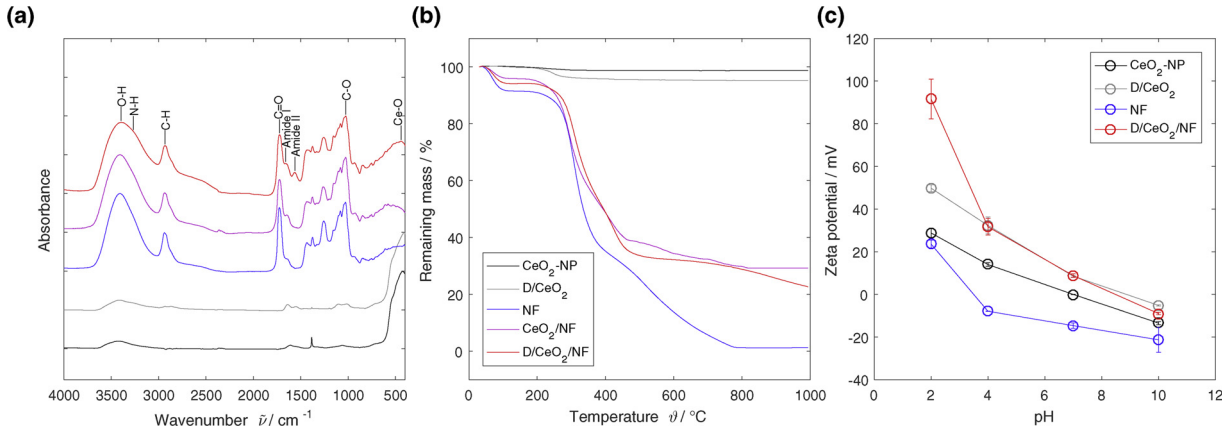


**Fig. 2.** (a) FTIR spectra, (b) TGA curves, and (c) pH dependent zeta potentials of $CeO_2$-NPs, D/$CeO_2$, NF, $CeO_2$/NF, and D/$CeO_2$/NF nanocomposites.

**Table 1**
Characterization of different samples.

| Sample | Abbreviation | Mass fraction $w$ of $CeO_2$ (%)* | Diameter (nm) | Experimental $a_{BET}$ ($m^2$ $g^{-1}$) | Calculated $a_{calc}$ ($m^2$ $g^{-1}$) | $q_e$ (mg $g^{-1}$)# |
|---|---|---|---|---|---|---|
| Ceria nanoparticles | $CeO_2$-NPs | 100 | 139 ± 2† (18.2)‡ | 45.6 | 6.0 | 83.8 ± 5.4 |
| Dendrimer treated $CeO_2$-NPs | D/$CeO_2$ | 96.3 | 167 ± 31† (21.4)‡ | 38.8 | 5.0 | 93.8 ± 5.1 |
| Pul/PVA/PAA nanofibers | NF | – | 548 ± 148§ | 3.6 | 5.3 | 6.8 ± 2.1 |
| Ceria coated nanofibers | $CeO_2$/NF | 29.2 | 771 ± 182§ | 5.3 | 6.7 | 101.1 ± 1.5 |
| Dendrimer treated ceria coated nanofibers | D/$CeO_2$/NF | 22.7 | 592 ± 139§ | 5.0 | 4.4 | 179.4 ± 1.1 |

* Extracted from TGA results.
† Based on DLS.
‡ Based on BET (spherical model, density ρ($CeO_2$) = 7.22 g $cm^{-3}$).
§ Based on SEM images.
# For general conditions see Fig. 3; for $CeO_2$-NPs, $CeO_2$/NF, and D/$CeO_2$: equivalent mass concentration of $CeO_2$ with respect to D/$CeO_2$/NF; for NF: γ(NF) = 100 mg $l^{-1}$.

by the size increase with time (Fig. S5).

### 3.2. Batch Cr(VI) adsorption

#### 3.2.1. Effect of supporting $CeO_2$-NPs and dendrimer treatment

The Cr(VI) adsorption efficiency of the D/$CeO_2$/NF nanocomposite was investigated by its equilibrium adsorption capacity with free $CeO_2$-NPs, dendrimer treated nanoparticles (D/$CeO_2$) and nanoparticles immobilized on the nanofiber mat ($CeO_2$/NF) as shown in Table 1. $CeO_2$-NPs had a Cr(VI) adsorption capacity of $q$($CeO_2$-NPs) = 83.8 mg $g^{-1}$ which can be due to their high surface area as reported in previous studies [2,43–45]. Dendrimer treatment of free nanoparticles increased the capacity of $CeO_2$-NPs to 93.8 mg $g^{-1}$ (12% increase). However ceria coated nanofibers ($CeO_2$/NF) had a better adsorption capacity ($q$($CeO_2$/NF = 101.1 mg $g^{-1}$) due to the presence of the unbiased support ($q$(NF) = 6.8 mg $g^{-1}$) which prevented agglomeration during the adsorption process. Surface treatment of $CeO_2$/NF with dendrimer finally rendered a highly efficient adsorbent with $q$(D/$CeO_2$/NF) = 179.4 mg $g^{-1}$ (77% increase). This significant increase was a direct consequence of the immobilization of the $CeO_2$-NPs on the nanofiber support, which kept the surface of all immobilized $CeO_2$-NPs accessible. Free $CeO_2$-NPs in contrary tended to agglomerate during dendrimer treatment as was seen in the increased particle size of 167 nm (21% increase) with the effect of less accessible surface.

#### 3.2.2. Effect of solution pH

Since pH is the most important factor in determining the charge density of the adsorbent and the heavy metal analyte in solution, it can affect the adsorption process remarkably as shown in Fig. 3a. An acidic environment increases the number of ammonium (-$NH_3^+$) groups on the surface of the nanocomposite which will adsorb Cr(VI) ions through electrostatic interaction [27]. The Cr(VI) ions exist in various forms such as $HCrO_4^-$, $Cr_2O_7^{2-}$, or $CrO_4^{2-}$ [46]. Their chemical speciation depends on pH and condensation equilibria as illustrated by the following

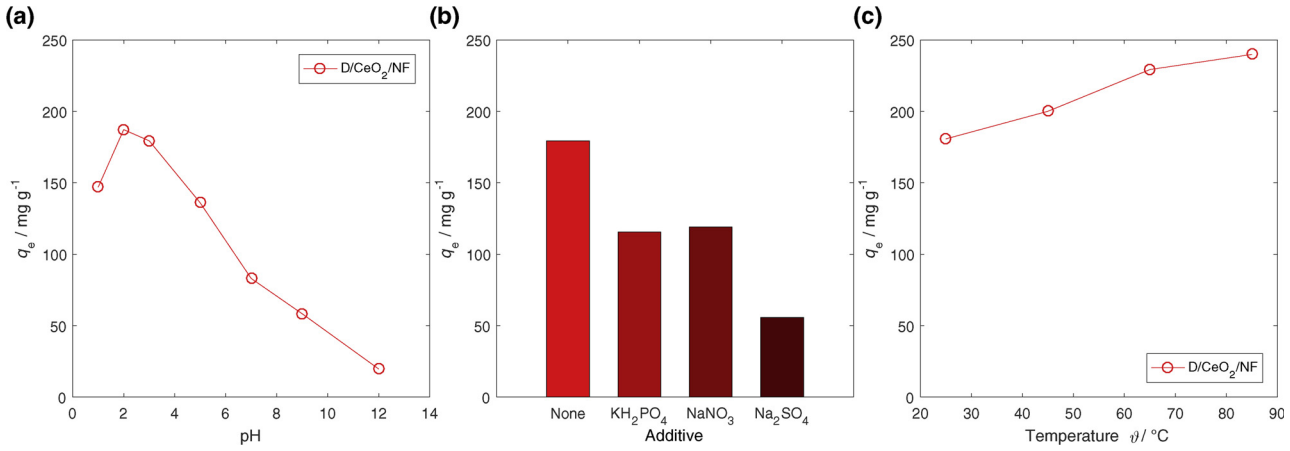


**Fig. 3.** Effect of (a) pH, (b) added ions and (c) temperature, on the adsorption capacity $q_e$ of D/$CeO_2$/NF. General conditions: $\gamma$(D/$CeO_2$/NF) = 167 mg $l^{-1}$, $\gamma_0$(Cr (VI)) = 50 mg $l^{-1}$, $\vartheta$ = 25 °C, pH = 3, $t$ = 8 h.

reactions [47,48]:

$$H_2CrO_4 \rightleftharpoons H^+ + HCrO_4^-, K_1 = 10^{0.26}\ mol/L \quad (4)$$

$$Cr_2O_7^{2-} + H_2O \rightleftharpoons 2\,HCrO_4^-, K_2 = 10^{-2.2}\ mol/L \quad (5)$$

$$HCrO_4^- \rightleftharpoons H^+ + CrO_4^{2-}, K_3 = 10^{-5.9}\ mol/L \quad (6)$$

At pH > 7, $CrO_4^{2-}$ is the dominating species while $Cr_2O_7^{2-}$ is the most stable Cr(VI) ion at lower pH. The increasing number of $NH_3^+$ groups at lower pH allows more electrostatic interactions with the negatively charged Cr(VI) ions with a positive effect on the adsorption capacity, Fig. 3a. The adsorption capacity decreased at high pH due to a neutral or negatively charged surface of the adsorbent. In addition, at basic conditions, large numbers of $OH^-$ groups are in the solution which competes with Cr(VI) ions for the active sites [49,50]. At very acidic pH, $H_2CrO_4$ becomes the dominant Cr(VI) species. This fact explains the lower removal capacity in a very acidic environment (pH < 2) since there is no electrostatic attraction between $H_2CrO_4$ and $NH_3^+$ groups.

According to different reports, most of the effluent from chromium industries is highly acidic and a highly effective adsorbent which is completely stable in low pH range would be a great advantage and industrially applicable [51,52].

### 3.2.3. Effect of the presence of other anions

Wastewaters of different factories contain various kinds of anions which can compete with the Cr(VI) ions in the adsorption process. Here the competing effect of $NO_3^-$, $SO_4^{2-}$, and $H_2PO_4^-$ as representative anions was investigated. Competing anions can reduce the Cr(VI) adsorption tendency as shown in Fig. 3b. Cr(VI) adsorption capacity reduces in the order of $NO_3^- < H_2PO_4^- < SO_4^{2-}$. Since the $Z/r$ (charge/radius) value of $SO_4^{2-}$ is bigger, the tendency of adsorption on active sites of D/$CeO_2$/NF is higher and less Cr(VI) will be adsorbed. On the other hand, in basic environment, $H_2PO_4^-$ will be transformed to $HPO_4^{2-}$ and $PO_4^{3-}$ ions which have a higher charge density than $NO_3^-$ resulting in a lower adsorption capacity for Cr(VI). The same results are reported in previous studies [27,53].

### 3.2.4. Effect of temperature

Fig. 3c shows an increasing adsorption capacity at higher temperature, which was also observed in other studies on Cr(VI) adsorption [4,27,54–56]. The positive temperature effect indicates a positive entropy ($\Delta S^\circ_{ad}$) of adsorption and it is studied in detail by the following equilibrium isotherms.

## 3.3. Continuous Cr(VI) adsorption in a fixed bed column

Only a few examples of applying electrospun nanofibers as adsorbents in fixed bed columns have been reported [54,57,58]. Technical limitations are given in the way of packing columns with nanofibers, in wall slipping effects, and in high differential pressure. Here we prepared fixed bed columns with thin beds comprised of one to three layers of nanofiber mats and we investigated them for the continuous adsorption of Cr(VI). The corresponding breakthrough curves are shown in Fig. 5. D/$CeO_2$/NF was more effective in retaining Cr(VI) than NF and the breakthrough point was successfully shifted to larger flow volumes by increasing the amount of bed material. The experimental data were fitted using the Thomas model [59] and equilibrium adsorption capacities $q_e$ between 54 and 79 mg $g^{-1}$ were obtained. For batch experiments, $q_e$ ($\gamma$(Cr(VI)) = 5 mg $l^{-1}$) was 50 ± 34 mg $g^{-1}$, according to the modified Freundlich isotherm, which is discussed in the modelling section. The corresponding Thomas rate constants $k_{Th}$ were between 0.04 and 0.07 l $mg^{-1}$ $min^{-1}$. Further details on the Thomas model are given in Fig. S6 and Table S1, Supporting information. Our data indicate that nanofiber mats such as D/$CeO_2$/NF can indeed be applied as stationary phase in fixed bed columns. Hardick et al. presented an operation scheme to simulate moving bed columns for continuous downstream processing using several fixed bed nanofiber based columns [57]. However, to overcome the intrinsic limitations of high differential pressure and stable column packing, alternative nanofiber based materials such as nanofiber based aerogels should be considered. We could recently demonstrate the continuous operation of such a nanofiber aerogel based fixed bed column for dye adsorption [18].

## 3.4. Regeneration and reusability

As one of the most fundamental issues, the cost effectiveness of D/$CeO_2$/NF was investigated by evaluating the regeneration ability of the nanocomposite. Different solutions for desorption process were used as presented in Fig. 4a. It shows that by using basic solution, 95% of chromium ions were desorbed which is favorable for desorption. According to Fig. 4b, a decrease of 12% in adsorption capacity is observed in the first cycle which increases in the following cycles to reach 28.3% at the fifth cycle.

Regeneration and reusability will also be crucial in cutting down the costs of using nanofiber based composites for water remediation applications. While large scale electrospinning is technically feasible these days [60], replacing $CeO_2$ with $TiO_2$ or silica and the dendrimer with polyethylenimine may also be considered to reduce the costs of D/$CeO_2$/NF.

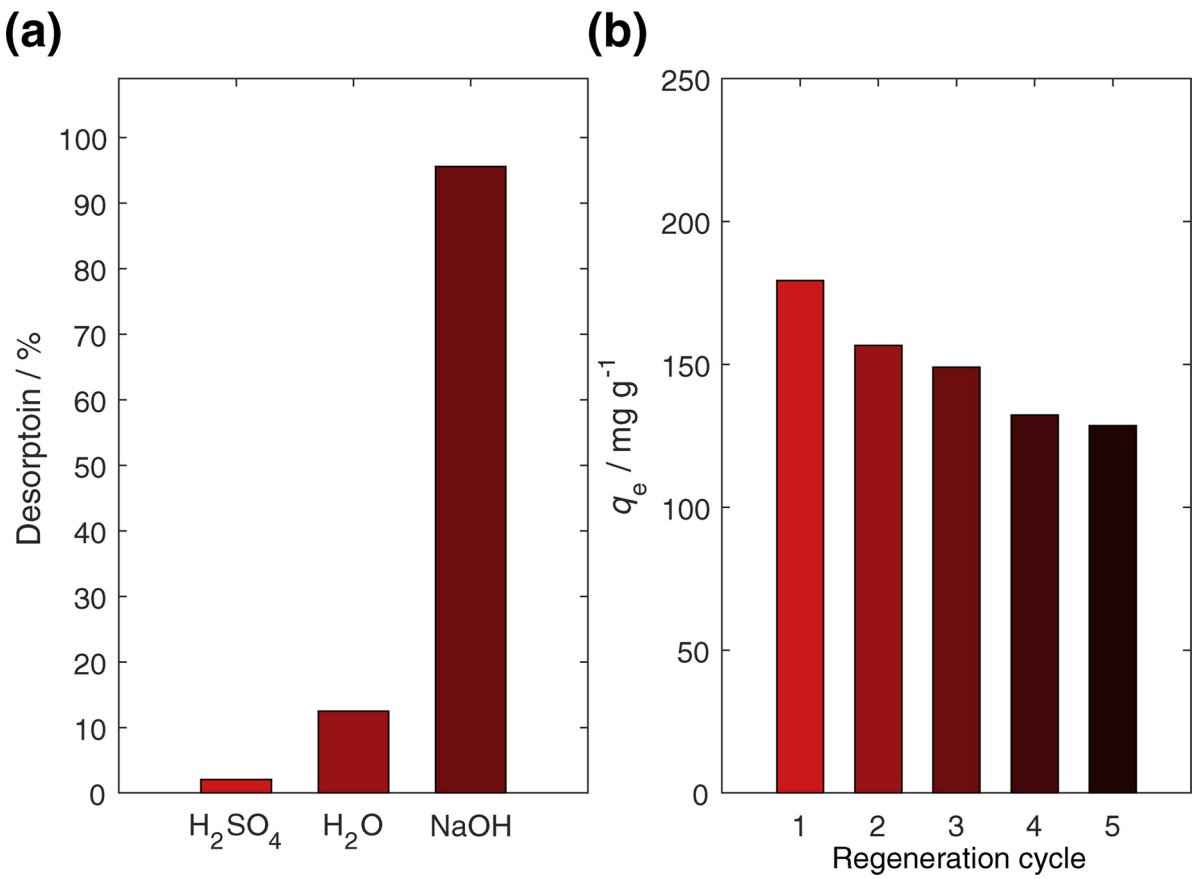


**Fig. 4.** (a) Desorption of Cr(VI) ions using $H_2SO_4$ ($c$ = 1 M), $H_2O$, and NaOH ($c$ = 0.1 M); (b) regeneration of D/$CeO_2$/NF.

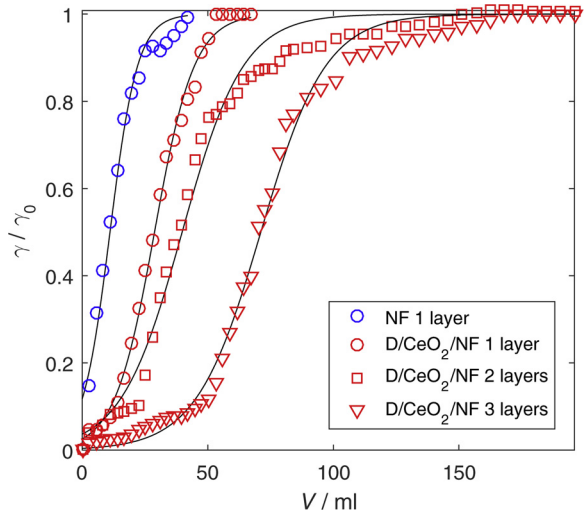


**Fig. 5.** Breakthrough curves for Cr(VI) using NF and D/$CeO_2$/NF, $\gamma_0$(Cr (VI)) = 5 mg l$^{-1}$.

### 3.5. Modelling

#### 3.5.1. Equilibrium isotherm models

Adsorption isotherm study gives an idea about the mechanism and the relationship between the adsorbent and adsorbate at equilibrium to estimate the maximum adsorption capacity of the adsorbent. Effect of the Cr(VI) concentration on adsorption was investigated and the data were analyzed using Langmuir and Freundlich models (Eqs. (7) and (9)) as well as a modified Langmuir model, Eq. (8), [61]:

$$\text{Langmuir: } q_e = q_{max}\frac{K_L\gamma_e}{1+K_L\gamma_e} \quad (7)$$

$$\text{Modified Langmuir: } q_e = q_{max}\frac{K_{ML}\gamma_e}{\gamma_s + (K_{ML}-1)\gamma_e} \quad (8)$$

$$\text{Freundlich: } q_e = K_F\gamma_e^{1/n} \quad (9)$$

Where $\gamma_e$ (mg l$^{-1}$) is the equilibrium mass concentration of Cr(VI) in solution, $\gamma_s$ (mg l$^{-1}$) is the mass concentration of saturated Cr(VI), $q_e$ (mg g$^{-1}$) and $q_{max}$ (mg g$^{-1}$) are the adsorption capacity at equilibrium and the maximum adsorption capacity per mass of nanocomposite. $K_L$ (l mg$^{-1}$) and $K_F$ (mg g$^{-1}$ (l mg$^{-1}$)$^{1/n}$) are constants for the Langmuir and the Freundlich isotherms, respectively, and $n$ is related to the adsorption intensity of the adsorbents [43,62]. The modified Langmuir isotherm does explicitly account for the chemical potential of the dissolved Cr (VI) ions in the desorption process by introducing $\gamma_s$ and the constant $K_{ML}$ is dimensionless. This allows also the direct determination of the thermodynamic parameters of adsorption, the Gibbs energy ($\Delta G^\circ_{ad}$), enthalpy ($\Delta H^\circ_{ad}$) and entropy of adsorption [61].

The fitting results are shown in Table 2 and Fig. 6a. All three isotherms are applicable for the system but by comparing the relative root mean square deviation (*RRMSD*), it was found that Langmuir and modified Langmuir isotherm (both 3.9% ≤ *RRMSD* ≤ 12.5%) are fitting better than the Freundlich model (15.4% ≤ *RRMSD* ≤ 19.1%) indicating monolayer adsorption of Cr(VI).

The maximum adsorption capacity of the new PAMAM based nanocomposite D/$CeO_2$/NF ($q_{max}$ = 847 mg g$^{-1}$) is compared with many different results reported previously using similar materials, Fig. 6b. So far, D/$CeO_2$/NF is outmatching the Cr(VI) adsorption capacity of other materials. The highest reported absorption capacity for a PAMAM based material is 378 mg g$^{-1}$ [27]. Based on the number of functional groups and assuming $Cr_2O_7^{2-}$ adsorption as the dominant species, the upper limit

**Table 2**
Adsorption isotherm parameters obtained from the Langmuir, modified Langmuir, and Freundlich models of Cr(VI) adsorption by D/$CeO_2$/NF (For conditions see Fig. 3, fitting statistics are given in Table S2).

| | Langmuir | | Modified Langmuir | | | Freundlich | |
|---|---|---|---|---|---|---|---|
| $\vartheta$ (°C) | $q_{max}$ (mg $g^{-1}$) | $K_L$ (l $mg^{-1}$) | $q_{max}$ (mg $g^{-1}$) | $K_M$ (-) | $\gamma_s$ (mg $l^{-1}$) | $n$ (-) | $K_F$ (mg $g^{-1}$ (l $mg^{-1}$)$^{1/n}$) |
| 25 | 847 ± 21 | 0.012 ± 0.001 | 845 ± 21 | 432 ± 41 | 34640 | 2.8 ± 0.4 | 75 ± 26 |
| 45 | 873 ± 59 | 0.014 ± 0.004 | 871 ± 58 | 930 ± 230 | 64340 | 2.9 ± 0.8 | 86 ± 52 |
| 65 | 855 ± 87 | 0.022 ± 0.09 | 855 ± 87 | 2400 ± 1100 | 117400 | 3.3 ± 0.9 | 114 ± 59 |
| 85 | 866 ± 99 | 0.029 ± 0.015 | 866 ± 99 | 4800 ± 2400 | 165000 | 3.6 ± 1.0 | 144 ± 65 |

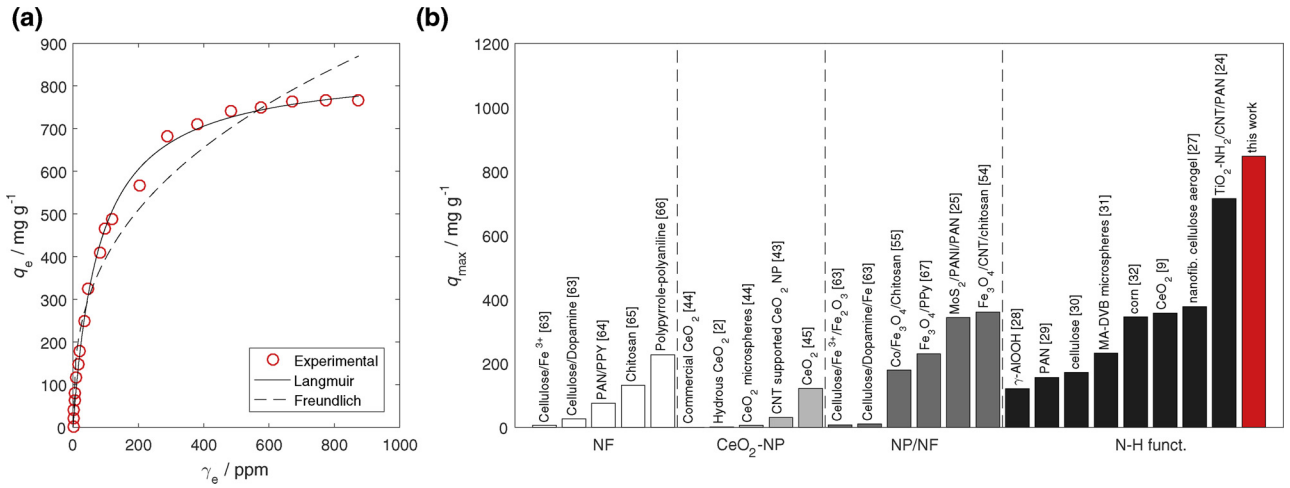


**Fig. 6.** Modelling of (a) adsorption isotherms (note, that the modified Langmuir isotherm is visually identical with the Langmuir isotherm) for D/$CeO_2$/NF, and (b) comparing maximum adsorption capacity $q_{max}$ of different adsorbents from the literature [2,9,24,25,27–32,43–45,54,55,63–67] with D/$CeO_2$/NF (this work).

**Table 3**
Thermodynamic parameters of Cr(VI) adsorption by D/$CeO_2$/NF (For conditions see Fig. 3).

| $\Delta H^\circ_{ad}$ (kJ $mol^{-1}$) | $\Delta S^\circ_{ad}$ (kJ $mol^{-1}$ $K^{-1}$) | $\Delta G^\circ_{ad}$ (kJ $mol^{-1}$) | | | |
|---|---|---|---|---|---|
| | | 25 °C | 45 °C | 65 °C | 85 °C |
| 37 ± 10 | 0.17 ± 0.03 | −15.0 ± 0.2 | −18.1 ± 0.7 | −22.1 ± 1.3 | −25.2 ± 1.6 |

**Table 4**
Kinetic parameters for Cr(VI) adsorption by D/$CeO_2$/NF according to pseudo first order, pseudo second order, and intra particle diffusion model (For conditions see Fig. 3, fitting statistics are given in Table S3).

| Model | Parameter | Quantity |
|---|---|---|
| Experimental equilibrium capacity | $q_{e,\ exp}$ (mg $g^{-1}$) | 179.4 ± 1.1 |
| Pseudo first order | $q_{e,\ 1st}$ (mg $g^{-1}$) | 167 ± 8 |
| | $k_1$ ($min^{-1}$) | 0.032 ± 0.007 |
| Pseudo second order | $q_{e,\ 2nd}$ (mg $g^{-1}$) | 184 ± 5 |
| | $k_2 \times 10^{-4}$ (g $mg^{-1}$ $min^{-1}$) | 2.3 ± 0.4 |
| Intra-particle diffusion | $k_{bl}$ (mg $g^{-1} min^{-\frac{1}{2}}$) | 19 ± 2 |
| | $k_{ip}$ (mg $g^{-1} min^{-\frac{1}{2}}$) | 3.5 ± 0.3 |
| | $I$ (mg $g^{-1}$) | 109 ± 5 |

for the adsorption capacity of PAMAM 3.0 should be 1445 mg $g^{-1}$. Here, we found a PAMAM 3.0 concentration of 599 mg $g^{-1}$ for D/$CeO_2$/NF. Therefore we can expect a $q_{max}$ of 866 mg $g^{-1}$. The difference between this hypothetical $q_{max}$ and the experimental $q_{max}$ = 847 mg $g^{-1}$ can be attributed to incomplete coverage and the supporting structure, which is less effective in Cr(VI) adsorption, see also Table 1.

### 3.5.2. Thermodynamic parameters of adsorption

In order to evaluate thermodynamic parameters of the adsorption process, the effect of temperature on adsorption was investigated between 25 °C and 85 °C as shown in Fig. S7. Gibbs energy, enthalpy and entropy of adsorption were calculated from the modified Langmuir constant $K_{ML}$ using Eqs. (10) and (11).

$$\Delta G^\circ_{ad} = -RT\ln(K_{ML}) \quad (10)$$

$$\ln(K_{ML}) = \frac{\Delta S^\circ_{ad}}{R} - \frac{\Delta H^\circ_{ad}}{RT} \quad (11)$$

Where $R$ (J $mol\ K^{-1}$) is the molar gas constant and $T$ (K) is the absolute temperature.

As shown in Fig. S7, the adsorption affinity of D/$CeO_2$/NF is becoming higher at higher temperature which reveals a process with positive entropy of adsorption ($\Delta S^\circ_{ad}$ = 170 ± 30 J $mol^{-1}$ $K^{-1}$) rendering the overall adsorption process spontaneous despite its endothermic enthalpy of adsorption ($\Delta H^\circ_{ad}$ = 37 ± 10 kJ $mol^{-1}$), see Table 3. The positive $\Delta S^\circ_{ad}$ during the adsorption process can be understood by increasing the degree of freedom of solvent cage $H_2O$ molecules surrounding the dissolved Cr(VI) ions as well as by releasing $H_2O$ molecules that are bound to the adsorption sites of the ammonium groups of the nanocomposite. Overall, the highly negative $\Delta G^\circ_{ad}$ shows the effectiveness of D/$CeO_2$/NF for absorbing Cr(VI) ions. Similar results are reported for other Cr(VI) adsorption processes [68].

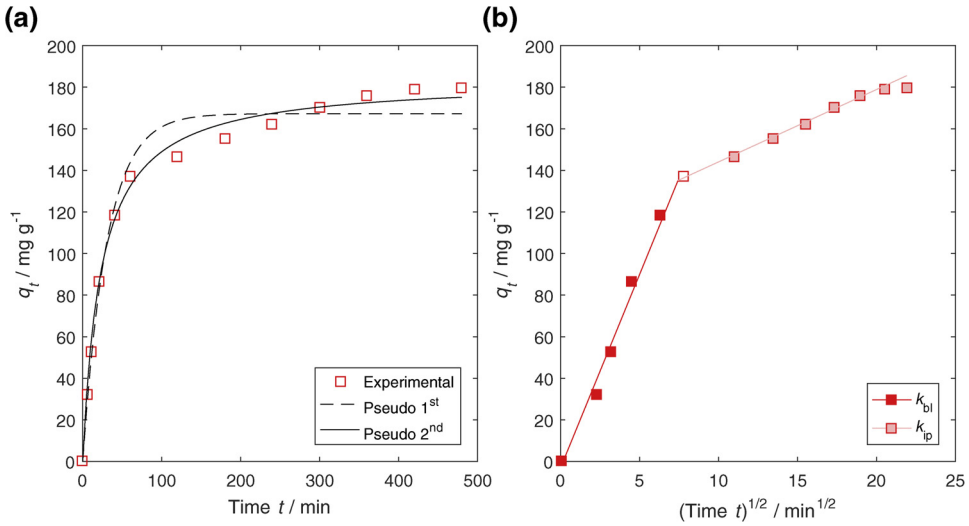


**Fig. 7.** Modelling (a) pseudo first and second order kinetics, and (b) boundary layer and intra-particle diffusion for Cr(VI) adsorption by D/$CeO_2$/NF. For conditions see Fig. 3.

*3.5.3. Adsorption kinetics*

To understand the adsorption mechanisms (chemical interaction, mass transfer, and diffusion control), different kinetic models (pseudo-first-order, pseudo-second-order and intra-particle diffusion) were used. The pseudo-first-order adsorption model is given by Eq. (12):

$$q_t = q_e(1 - \exp(-k_1 t)) \tag{12}$$

Where $k_1$ is the rate constant of pseudo first order adsorption and $q_t$ is the Cr(VI) adsorption capacity at time $t$.

The linear form of the pseudo-second-order model is given by Eq. (13):

$$q_t = \frac{k_2 {q_e}^2 t}{1 + k_2 q_e t} \tag{13}$$

Where $k_2$ is the rate constant of pseudo second order adsorption.

The possibility of intra-particle diffusion during the adsorption process is investigated using the intra-particle diffusion model as:

$$q_t = kt^{1/2} + I \tag{14}$$

Where $k$ is the diffusion rate constant and $I$ is a constant related to the boundary layer thickness: the larger the value of $I$, the greater the boundary layer effect will be. The "bl" and "ip" indices in Table 4 represent the boundary layer and intra-particle diffusion, respectively [69]. Comparing the results presented in Fig. 7a and Table 4, the pseudo-first-order model fits the data ($RRMSD$ = 7.8%), but the pseudo-second-order kinetic model can predict the experimental equilibrium adsorption capacity better ($RRMSD$ = 3.7%). Since with agitation of the solution, migration of Cr(VI) ions to the surface of adsorbent is fast enough, pseudo-second-order kinetic shows that the rate-controlling mechanism is chemisorption with electrostatic bonds. The same results are reported in similar studies [29,70]. To identify the diffusion mechanism, the intra-particle diffusion model was used as presented in Fig. 7b. It is clear that the adsorption has more than one step, involving a very fast adsorption on the surface of the nanocomposite with its high amount of tertiary ammonium groups followed by other slow processes which can be referred to adsorption and diffusion into nanoparticles and nanofibers and encapsulation of Cr(VI) ions.

## 4. Conclusion

In this study, a surface enriched nanocomposite of ceria covered electrospun nanofibers with a high amount of active amine groups on the surface was synthesized. The specific surface area was determined by BET measurements and geometric models based on the diameter of the nanofiber support and the ceria nanoparticles are able to predict the order of magnitude of the specific surface area. The nanocomposite is well suited for Cr(VI) adsorption in acidic solutions due to protonation of the amine groups. The achieved specific adsorption capacity $q_{max}$(D/$CeO_2$/NF) = 847 mg g$^{-1}$ is the highest value reported in similar studies so far. The adsorption process is endothermic and pseudo-second-order kinetic fit the kinetic data well indicating a chemical adsorption process with electrostatic bonds between ammonium groups and Cr(VI) ions. Since several adsorption-desorption cycles are applicable, the nanocomposite can be considered as an efficient and cost effective alternative adsorbent for Cr(VI) in environmental remediation.

## Acknowledgement

We thank Dr. Nicola Zucchetto for the BET measurements.

## Appendix A. Supplementary data

Supplementary material related to this article can be found, in the online version, at doi:https://doi.org/10.1016/j.jece.2018.102817.

## References

[1] K. Sirvidya, K. Mohanty, Biosorption of hexavalent chromium from aqueous solutions by Catla catla scales: equilibrium and kinetics studies, Chem. Eng. J. 155 (2009) 666–673.
[2] A.B. Albadarin, Z. Yang, C. Mangwandi, Y. Glocheux, G. Walker, M.N.M. Ahmed, Experimental design and batch experiments for optimization of Cr(VI) removal from aqueous solutions by hydrous cerium oxide nanoparticles, Chem. Eng. Res. Des. 92 (2014) 1354–1362.
[3] M. Costa, Potential hazards of hexavalent chromate in our drinking water, Toxicol. Appl. Pharmacol. 188 (2003) 1–5.
[4] A. Razzaz, S. Ghorban, L. Hosayni, M. Irani, M. Aliabadi, Chitosan nanofibers functionalized by TiO2 nanoparticles for the removal of heavy metal ions, J. Taiwan Instit. Chem. Eng. 58 (2016) 333–343.
[5] K. Anupam, S. Dutta, C. Bhattacharjee, S. Datta, Adsorptive removal of chromium (VI) from aqueous solution over powdered activated carbon: optimization through response surface methodology, Chem. Eng. J. 173 (2011) 135–143.
[6] M. Hua, S. Zhang, B. Pan, W. Zhang, L. Lv, Q. Zhang, Heavy metal removal from water/wastewater by nanosized metal oxides: a review, J. Hazard. Mater. 211–212 (2012) 317–331.
[7] X. Qu, P.J.J. Alvarez, Q. Li, Application of nanotechnology in water and wastewater treatment, Water Res. 47 (2013) 3931–3946.
[8] F. Xu, G. Cheng, S. Song, Y. Wei, R. Chen, Insights into promoted adsorption capability of layered BiOCl nanostructures decorated with TiO2 nanoparticles, ACS Sustain. Chem. Eng. 4 (2016) 7013–7022.
[9] S. Mandal, S.S. Mahapatra, R.K. Patel, Enhanced removal of Cr(VI) by cerium oxide polyaniline composite: optimization and modeling approach using response surface methodology and artificial neural networks, J. Environ. Chem. Eng. 3 (2015) 870–885.

[10] R. Koole, E. Groeneveld, D. Vanmaekelbergh, A. Meijerink, C. de mello Donega, Size effects on semiconductor nanoparticles, in: C. de Mello Donega (Ed.), Nanoparticles, Springer, Berlin, 2014, pp. 13–51.
[11] C. Wan, J. Li, Facile synthesis of well-dispersed superparamagnetic γ-Fe2O3 nanoparticles encapsulated in three-dimensional architectures of cellulose aerogels and their applications for Cr(VI) removal from contaminated water, ACS Sustain. Chem. Eng. 3 (2015) 2142–2152.
[12] T. Pradeep, Anshup, Nobel metal nanoparticles for water purification: a critical review, Thin Solid Films 517 (2009) 6441–6478.
[13] Y. Lu, Z. Wu, M. Li, Q. Liu, D. Wang, Hydrophilic PVA-co-PE nanofiber membrane functionalized with iminodiacetic acid by solid-phase synthesis for heavy metal ions removal, React. Funct. Polym. 82 (2014) 98–102.
[14] A. Dastbaz, A.R. Keshtkar, Adsorption of Th4+, U6+, Cd2+, and Ni2+ from aqueous solution by a novel modified polyacrylonitrile composite nanofiber adsorbent prepared by electrospinning, Appl. Surf. Sci. 293 (2014) 336–344.
[15] X. Li, C. Zhang, R. Zhao, X. Lu, X. Xu, X. Jia, C. Wang, L. Li, Efficient adsorption of gold ions from aqueous systems with thioamide-group chelating nanofiber membranes, Chem. Eng. J. 229 (2013) 420–428.
[16] F. Deuber, S. Mousavi, L. Federer, C. Adlhart, Amphiphilic nanofiber-based aerogels for selective liquid absorption from electrospun biopolymers, Adv. Mater. Interfaces 4 (2017) 1700065.
[17] F. Deuber, S. Mousavi, M. Hofer, C. Adlhart, Tailoring pore structure of ultralight electrospun sponges by solid templating, ChemistrySelect 1 (2016) 5595–5598.
[18] S. Mousavi, F. Deuber, S. Petrozzi, L. Federer, M. Aliabadi, F. Shahraki, C. Adlhart, Efficient dye adsorption by highly porous nanofiber aerogels, Colloids Surf. A Physicochem. Eng. Asp. 547 (2018) 117–125.
[19] F. Deuber, S. Mousavi, L. Federer, M. Hofer, C. Adlhart, Exploration of ultralight nanofiber aerogels as particle filters: capacity and efficiency, ACS Appl. Mater. Interfaces 10 (2018) 9069–9076.
[20] R. Zhao, Y. Wang, X. Li, B. Sun, Y. Li, H. Ji, J. Qiu, C. Wang, Surface activated hydrothermal carbon-coated electrospun PAN fiber membrane with enhanced adsorption properties for herbicide, ACS Sustain. Chem. Eng. 4 (2016) 2584–2592.
[21] S. Zhao, O. Emery, A. Wohlhauser, M.M. Koebel, C. Adlhart, W.J. Malfait, Merging flexibility with superinsulation: machinable, nanofibrous pullulan-silica aerogel composites, Mater. Des. 160 (2018) 294–302.
[22] M. Khorram, A. Mousavi, N. Mehranbod, Chromium removal using adsorptive membranes composed of electrospun plasma-treated functionalized polyethylene terephthalate (PET) with chitosan, J. Environ. Chem. Eng. 5 (2017) 2366–2377.
[23] D. Morillo Martín, M. Faccini, M.A. García, D. Amantia, Highly efficient removal of heavy metal ions from polluted water using ion-selective polyacrylonitrile nanofibers, J. Environ. Chem. Eng. 6 (2018) 236–245.
[24] A. Mohamed, W.S. Nasser, T.A. Osman, M.S. Toprak, M. Muhammed, A. Uheida, Removal of Chromium (VI) from aqueous solutions using surface modified composite nanofibers, J. Colloid Interface Sci. 505 (2017) 682–691.
[25] J. Qiu, F. Liu, S. Cheng, L. Zong, C. Zhu, C. Ling, A. Li, Recyclable nanocomposite of flowerlike MoS2@Hybrid acid-doped PANI immobilized on porous PAN nanofibers for the efficient removal of Cr(VI), ACS Sustain. Chem. Eng. 6 (2017) 447–456.
[26] A.G.N. Wamba, G.P. Kofa, S.N. Koungou, P.S. Thue, E.C. Lima, G.S. dos Reis, J.G. Kayem, Grafting of Amine functional group on silicate based material as adsorbent for water purification: a short review, J. Environ. Chem. Eng. 6 (2018) 3192–3203.
[27] J. Zhao, X. Zhang, X. He, M. Xiao, W. Zhang, C. Lu, A super biosorbent from dendrimer poly amidoamine grafted cellulose nanofibril aerogels for effective removal of Cr(VI), J. Mater. Chem. A 3 (2015) 14703–14711.
[28] H. Zhang, P. Li, Z. Wang, W.W. Cui, Y. Zhang, Y. Zhang, S. Zheng, Y. Zhang, Sustainable disposal of Cr(VI): adsorption–reduction strategy for treating textile wastewaters with amino-functionalized boehmite hazardous solid wastes, ACS Sustain. Chem. Eng. 6 (2018) 6811–6819.
[29] M. Avila, T. Burks, F. Akhtar, M. Gothelid, P.C. Lansaker, M.S. Toprak, M. Muhammed, A. Uheida, Surface functionalized nanofibers for the removal of chromium(VI) from aqeous solutions, Chem. Eng. J. 245 (2014) 201–209.
[30] H. Zhu, Q. Kong, X. Cao, H. He, J. Wang, Y. He, Adsorption of Cr(VI) from aqueous solution by chemically modified natural cellulose, Desalin. Water Treat. 57 (2015) 20368–20376.
[31] W. Song, B. Gao, T. Zhang, X. Xu, X. Huang, H. Yu, Q. Yue, High- capacity adsorption of dissolved hexavalent chromium using amine- functionalized magnetic corn stalk composites, Bioresour. Technol. 190 (2015) 550–557.
[32] H. Wang, X. Xu, Z. Ren, B. Gao, Removal of phosphate and chromium (VI) from liquids by an amine-crosslinked nano-Fe3O4 biosorbent derived from corn straw, RSC Adv. 6 (2016) 47237–47248.
[33] H. Li, Z. Zhang, X. Ma, M. Hu, X. Wang, P. Fan, Synthesis and characterization of epoxy resin modified with nano-SiO2 and γ-glycidoxypropyltrimethoxy silane, Surf. Coat. Technol. 201 (2007) 5269–5272.
[34] S. Chandra, S. Mehta, S. Nigam, D. Bahadur, Dendritic magnetite nanocarriers for drug delivery applications, New J. Chem. 34 (2010) 648–655.
[35] Y. Chang, X. Meng, Y. Zhao, M. Zhu, Y. Li, X. Chen, J. Wang, Novel water-soluble and pH-responsive anticancer drug nanocarriers: doxorubicin–PAMAM dendrimer conjugates attached to superparamagnetic, J. Colloid Interface Sci. 363 (2011) 403–409.
[36] J.J. Stanger, N. Tucker, N. Buunk, Y.B. Truong, A comparison of automated and manual techniques for measurement of electrospun fibre diameter, Polym. Test. 40 (2014) 4–12.
[37] N. Bendixen, S. Losert, C. Adlhart, M. Lattuada, A. Ulrich, Membrane-particle interactions in an asymmetric flow field flow fractionation channel studied with titanium dioxide nanoparticles, J. Chromatogr. A 1334 (2014) 92–100.
[38] A.I. Vogel, A Text-book of Quantitative Inorganic Analysis Including Elementary Instrumental Analysis, 3rd ed., John Wiley and Sons, New York, 1961.
[39] B. Krishnakumar, T. Imae, Chemically modified novel PAMAM-ZnO nanocomposite: synthesis, characterization and photocatalytic activity, Appl. Catal. A Gen. 486 (2014) 170–175.
[40] F. Kayaci, Z. Aytac, T. Uyar, Surface modification of electrospun polyester nanofibers with cyclodextrin polymer for the removal of phenanthrene from aqueous solution, J. Hazard. Mater. 261 (2013) 286–294.
[41] Y.J. Ryu, H.Y. Kim, K.H. Lee, H.C. Park, D.R. Lee, Transport properties of electrospun nylon 6 nonwoven mats, Eur. Polym. J. 39 (2003) 1883–1889.
[42] A. Maleki, B. Hayati, F. Najafi, F. Gharibi, S.W. Joo, Heavy metal adsorption from industrial wastewater by PAMAM/TiO2 nanohybrid: preparation, characterization and adsorption studies, J. Mol. Liq. 224 (2016) 95–104.
[43] Z.-C. Di, J. Ding, X.-J. Peng, Y.-H. Li, Z.-K. Luan, J. Liang, Chromium adsorption by aligned carbon nanotubes supported ceria nanoparticles, Chemosphere 62 (2006) 861–865.
[44] H. Xiao, Z. Ai, L. Zhang, Nonaqueous sol-Gel snthesized Hierarchical CeO2 Nanocrystal microspheres as novel adsorbents for wastewater treatment, J. Phys. Chem. C 113 (2009) 16625–16630.
[45] S. Recillas, J. Colon, E. Casals, E. Gonzalez, V. Puntes, A. Sanchez, X. Font, Chromium VI adsorption on cerium oxide nanoparticles and morphology changes during the process, J. Hazard. Mater. 184 (2010) 425–431.
[46] R. Rakhunde, L. Deshpande, H.D. Juneja, Chemical speciation of chromium in water: a review, Crit. Rev. Environ. Sci. Technol. 42 (2012) 776–810.
[47] N.S. Chamberlin, R.V. Day, Technology of chrome reduction with sulfur dioxide, Proceedings of the Eleventh Purdue Insutrial Waster Water Conference (1957) 129–156.
[48] G. Naja, B. Volesky, The mechanism of metal cation and anion biosorption, in: P. Kotrba, M. Mackova, T. Macek (Eds.), Microbial Biosorption of Metals, Springer, Netherlands, Dordrecht, 2011, pp. 19–58.
[49] Y. Ku, I.-L. Jung, Photocatalytic reduction of Cr (VI) in aqueous solutions by UV irradiation with the presence of titanium dioxide, Water Res. 35 (2001) 135–142.
[50] M. Huang, S.B. Mishra, S. Liu, Waste glass Fiber fabric as a support for facile synthesis of microporous carbon to adsorb Cr(VI) from wastewater, ACS Sustain. Chem. Eng. 5 (2017) 8127–8136.
[51] J. Majumdar, B.K. Baruah, K. Dutta, Sources and characteristics of galvanizing industry effluent, J. Ind. Pollut. Control 23 (2007) 119–123.
[52] G. Moussavi, B. Barikbin, Biosorption of chromium(VI) from industrial wastewater onto pistachio hull waste biomass, Chem. Eng. J. 162 (2010) 893–900.
[53] L. Lv, J. He, M. Wei, D.G. Evans, Z. Zhou, Treatment of high fluoride concentration water by MgAl-CO3 layered double hydroxides: kinetic and equilibrium studies, Water Res. 41 (2007) 1534–1542.
[54] H. Beheshti, M. Irani, L. Hosseini, A. Rahimi, M. Aliabadi, Removal of Cr (VI) from aqeous solutions using chitosan/MWCNT/Fe3O4 composite nanofibers-batch and column studies, Chem. Eng. J. 284 (2016) 557–564.
[55] M. Aliabadi, Removal of Pb(II) and Cr(VI) ions from aqueous solutions using chitosan/cobalt farrite nanofibrous adsorbent, Fibers Polym. 17 (2016) 1162–1170.
[56] D.D. Xu, J.W. Lu, S. Yan, R. Xiao, Aminated EVOH nanofiber membranes for Cr(VI) adsorption from aqueous solution, RSC Adv. 8 (2018) 742–751.
[57] O. Hardick, S. Dods, B. Stevens, D.G. Bracewell, Nanofiber adsorbents for high productivity continuous downstream processing, J. Biotechnol. 213 (2015) 74–82.
[58] V. Sabourian, A. Ebrahimi, F. Naseri, M. Irani, A. Rahimi, Fabrication of chitosan/silica nanofibrous adsorbent functionalized with amine groups for the removal of Ni (ii), Cu(ii) and Pb(ii) from aqueous solutions: batch and column studies, RSC Adv. 6 (2016) 40354–40365.
[59] H.C. Thomas, Chromatography: a problem in kinetics, Ann. N. Y. Acad. Sci. 49 (1948) 161–182.
[60] C.J. Luo, S.D. Stoyanov, E. Stride, E. Pelan, M. Edirisinghe, Electrospinning versus fibre production methods: from specifics to technological convergence, Chem. Soc. Rev. 41 (2012) 4708–4735.
[61] S. Azizian, S. Eris, L.D. Wilson, Re-evaluation of the century-old Langmuir isotherm for modeling adsorption phenomena in solution, Chem. Phys. 513 (2018) 99–104.
[62] K.Y. Foo, B.H. Hameed, Insights into the modeling of adsorption isotherm systems, Chem. Eng. J. 156 (2010) 2–10.
[63] A.D. Dwivedi, N.D. Sanandiya, J.P. Singh, S.M. Husnain, K.H. Chae, D.S. Hwang, Y.-S. Chang, Tuning and characterizing nanocellulose interface for enhanced removal of dual-sorbate (AsV and CrVI) from water matrices, ACS Sustain. Chem. Eng. 5 (2016) 518–528.
[64] J. Wang, K. Pan, Q. He, B. Cao, Polyacrylonitrile/polypyrrole core/shell nanofiber mat for the removal of hexavalent chromium from aqueous solution, J. Hazard. Mater. 244–245 (2013) 121–129.
[65] L. Li, Y. Li, L. Cao, C. Yang, Enhanced chromium (VI) adsorption using nanosized chitosan fibers tailored by electrospinning, Carbohydr. Polym. 125 (2015) 206–213.
[66] M. Bhaumik, A. Maity, V.V. Srinivasu, M.S. Onyango, Removal of hexavalent chromium from aqueous solution using polypyrrole-polyaniline nanofibers, Chem. Eng. J. 181–182 (2012) 323–333.
[67] M. Bhaumik, A. Maity, V.V. Srinivasu, M.S. Onyango, Enhanced removal of Cr(VI) from aqueous solution using polypyrrole/Fe3O4 magnetic nanocomposite, J. Hazard. Mater. 190 (2011) 381–390.
[68] R.M. Schneider, C.F. Cavalin, M.A.S.D. Barros, C.R.G. Tavares, Adsorption of chromium ions in activated carbon, Chem. Eng. J. 132 (2007) 355–362.
[69] V. Fierro, V. Torne- fernandez, D. Montane, A. Celzard, Adsorption of phenol onto activated carbons having different textural and surface properties, Microporous Mesoporous Mater. 111 (2008) 276–284.
[70] Y. Khambhaty, K. Mody, S. Basha, B. Jha, Kinetics, equilibrium and thermodynamic studies on biosorption of hexavalent chromium by dead fungal biomass of marine Aspergillus niger, Chem. Eng. J. 145 (2009) 489–495.